CORA Cork Open Research Archive
Cartlann Taighde Oscailte Chorcaí

Title	Cavity-enhanced absorption detection of H2S in the near-infrared using a gain-switched frequency comb laser
Authors	Chandran, Satheesh;Mahon, Stephen;Ruth, Albert A.;Braddell, J.;Gutiérrez, M. D.
Publication date	2018-03-29
Original Citation	Chandran, S., Mahon, S., Ruth, A. A., Braddell, J. and Gutiérrez, M. D. (2018) 'Cavity-enhanced absorption detection of H2S in the near-infrared using a gain-switched frequency comb laser', Applied Physics B, 124(4), 63 (9pp). doi:10.1007/s00340-018-6931-z
Type of publication	Article (peer-reviewed)
Link to publisher's version	10.1007/s00340-018-6931-z
Rights	© 2018, Springer-Verlag GmbH Germany, part of Springer Nature. All rights reserved. This is a post-peer-review, pre-copyedit version of an article published in International Applied Physics B. The final authenticated version is available online at: https://doi.org/10.1007/s00340-018-6931-z
Download date	2026-10-07 15:28:44
Item downloaded from	https://hdl.handle.net/10468/6495

UCC
University College Cork, Ireland
Coláiste na hOllscoile Corcaigh

Cavity-Enhanced Absorption Detection of H_2S in the Near Infrared Using a Gain-switched Frequency Comb Laser

S. Chandran[1], S. Mahon[1,#], A.A. Ruth[1,*], J. Braddell[2], M.D. Gutiérrez[2]

[1]*Physics Department & Environmental Research Institute, University College Cork, Cork, Ireland*

[2] *Pilot Photonics Limited, Invent Centre, Dublin City University, Glasnevin, Dublin 9, Ireland*

Abstract

A custom-designed gain-switched frequency comb laser was passively coupled of to a medium finesse cavity in the region between 6346 cm^{-1} and 6354 cm^{-1} for the development of a prototype cavity enhanced absorption setup. The setup was applied to static gas detection of hydrogen sulfide at the parts per thousand level in a laboratory environment. A Fourier transform spectrometer was used for signal detection. The experimental performance of the setup was characterized in this proof-of-principle investigation; advantages, drawbacks and future scope of the approach are discussed in this article.

*Corresponding Author. Email: a.ruth@ucc.ie, Tel: +353-21-4902057, Fax: +353-21-4276949

#Current address: Scottish Microelectronics Centre, King's Buildings, Alexander Crum Brown Road, Edinburgh EH9 3FF, United Kingdom

1. Introduction

Among the many applications of frequency combs (FC) in metrology (e.g. optical clocks and low noise frequency synthesis) [1-3], combs have long been recognized as superior light sources for absorption spectroscopy [4-6]. FC lasers generate a large stable array of equally spaced, phase-coherent, narrow-band spectral lines. In excess of 10^5 comb lines can be produced with mode-locked short pulse lasers, with line spacing in the region of many 10s of MHz (depending on the comb laser's repetition rate [1]). The comb lines' narrow bandwidth is determined by the coherence time of the laser.

In many cases the spectral resolution in absorption experiments is however limited by the spectrometer used for detection. In these cases FCs are essentially broadband lasers which act as a "spectral ruler" [1]. To exploit the inherently high resolution of FCs, new detection schemes using virtually imaged phase arrays spectrometers [7-9], comb-cavity vernier approaches [10,11] and Fourier-transform based dual comb spectroscopy [12-17] have been established. Some of these methods were recently reviewed [18]. To enhance the sensitivity in absorption experiments, applications of FCs in conjunction with optically stable cavities covering a spectral range that is limited by the high reflectivity range of the cavity mirrors have been developed [19,20]. The key challenge of cavity-enhanced FC absorption spectroscopy is the coupling of the FC to the cavity by matching the comb lines to an appropriately designed mode structure of a high finesse cavity – different approaches to coupling and locking of FC lines to high finesse optical cavities have also been reviewed [21].

In contrast to developing ultimate instrumental limits, the approach to cavity-enhanced absorption detection in this work aims at experimental simplicity. The principle suitability of a custom-built gain-switched frequency comb (GSFC) laser in conjunction with a very modest optical cavity was examined without spectrally stabilizing or mode-matching the cavity. GSFCs are tunable FCs that are simple in design and significantly cheaper than mode locked femtosecond FC lasers [22]. They, however, do not deliver the finely spaced large number of comb lines and span a significantly smaller wavelength region (~typically a few nm). GSFCs are generated by the direct modulation of commercially available laser diodes, as a distributed feedback laser, with a radiofrequency (RF) sine wave. External optical injection in a master-slave laser configuration can be employed to generate narrow line widths and low intensity noise [23]. GSFCs can also be integrated as a

monolithic devices [24] (see conclusion & outlook). The approach is simple and cost-efficient, and enables wavelength tunability of the comb and the line spacing, but with a rather limited number of comb lines [22]. GSFC lasers are commonly used as benchtop units for optical telecommunication in the C-band [22]. Recently a dual comb GSFC setup was reported based on gain switching and optical injection locking [25], with potential applications of the dual comb architecture in the mid-IR or near UV. In Ref [25] the absorption feature of $H^{13}CN$ in the 1.5 µm region were reported.

The objective of this study was to simply tune more than one laser comb line to absorption features of an appropriate target gas (hydrogen sulfide, H_2S) and to achieve sensitivities below the combustion limit of the hazardous gas in the parts per thousand (ppTv) regime using a low finesse ($\mathcal{F}$~ 450) optical cavity without a mode matching schemes.

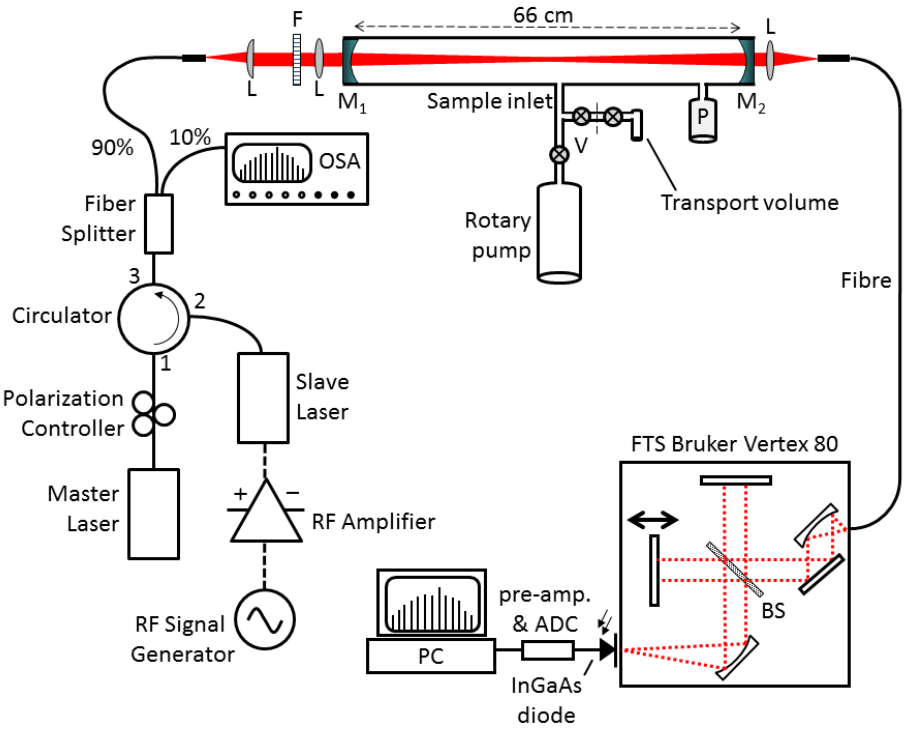

Fig. 1 Schematic of the experimental setup. Mirrors M_1 and M_2 are high-reflectivity dielectric mirrors (R~0.993) forming a medium finesse optical cavity with a length of 66 cm. L: Lenses used for collimation and light collection. P: Absolute Pressure gauge. V: Valves. RF: Radio Frequency (~10 GHz). ADC: Analog-to-Digital Converter. OSA: Optical Spectrum Analyzer.

2. Experiment

The schematic of the experimental setup is shown in Fig. 1. The main components of the GSFC laser were a tunable master laser (HP-8168F), a distributed feedback slave laser (Thorlabs, ITC-502), an radio frequency (RF) signal generator (HP-83751A), a biased RF amplifier (Aldetec, ALP-0618S430), a polarization controller, and a circulator. The slave laser was kept at a stable operating temperature by employing a thermoelectric cooler and a thermistor in the laser package. The (tunable) frequency of the master laser was slightly detuned (to higher energies) from that of the slave laser. Polarization controlled light from the master laser was injected via a circulator (ports 1 & 2) into the slave laser. The optical injection power was ≈3.1 mW (5 dBm). For a DC bias current of 45.1 mA the gain switching was achieved by continuously driving the slave laser above and below its laser threshold using an amplified sinusoidal RF signal. This created a train of pulses corresponding to an optical comb in the frequency domain. The (tunable) frequency of the RF generator hence determined the free spectral range of the FC, which in the present experiment was typically maintained at ~10 GHz (see Fig. 3). The absolute center frequency of the GSFC was controlled through the frequency of the master laser, which was tunable external cavity diode laser. In this experiment wavelength of the master laser was typically maintained at ~1574.8 nm (~6349.4 cm^{-1}); cp. Fig. 3. Overall the GSFC produced twenty phase-coherent, equally spaced comb lines with an individual spectral width of ~300 kHz [23] covering a range from 6346 to 6354 cm^{-1} (1575.8…1573.8 nm) in the near infra-red with an overall quasi-continuous integrated power close to ≈4 mW (6 dBm). For monitoring the GSFC emerging from port 3 of the circulator (Fig. 1), the light was split into two beams (ratio 90:10) and the less intense fraction of the beam was guided to an optical spectrum analyzer (OSA, Advantest Q8384). The main beam (90%) was collimated with a plano-convex (f ~ 25 mm) and a biconvex lens (f ~ 75 mm). The collimated light was guided into a stable optical cavity consisting of two plano-concave dielectric mirrors (diameter 25 mm, r = –200 cm, Layertec GmbH) at a distance of d = 66.0±0.1 cm. The modest reflectivity of the cavity mirrors of R = 0.993±0.001 was measured with a double-beam UV/Vis/NIR spectrometer (PerkinElmer, Lambda-1050). The optical cavity was enclosed by a stainless steel vacuum tube (diameter ~ 40 mm) which was fitted with an access port for evacuation and sample injection as schematically shown in Fig. 1. Before experiments the static gas cavity was evacuated by a rotary pump to ~ 0.1 mbar. The light exiting the cavity was collected with an achromatic lens and focused into a multimode light-guide (diameter 1.5 mm) which was

connected to the entrance aperture of a Fourier transform spectrometer (FTS, Vertex 80 with CaF_2 beam splitter, Bruker Ltd.). In the spectrometer an InGaAs photodiode was used to detect the light transmitted by the cavity. Using the Bruker OPUS software spectra were recorded with a spectral resolution of 0.08 cm^{-1} in an integration time of 120 s (corresponding to 4 scans per spectrum). This integration time was based on the optimum measured signal-to-noise ratio of the FC, established in a series of intensity stability measurements using the FTS and OSA.

Hydrogen sulfide (H_2S) (BOC Industrial Gases, >99.9%) was used as target gas in this proof-of-principle experiment. It is a poisonous and corrosive gas that can occur as a pollutant in industrial settings, such as oil refineries, production facilities involving petro-chemistry, gas processing plants and gas fields. Since it is heavier than air it can accumulate in badly ventilated areas and constitute a fire or explosion hazard due to its flammable nature [26]. The main source of H_2S as a natural atmospheric pollutant is from volcanic activity. The changes in the H_2S release rate from dormant volcanos in comparison to other trace species is used to monitor volcanic activity before potential eruptions [26]. Thus the spectroscopic detection of H_2S in industrial and environmental applications is of high relevance and motivated its usage in this GSFC application. High detection sensitivity was however not expected a priori, due to the comparatively small absorption cross-sections of H_2S in the spectral target region at ~6350 cm^{-1} and the modest mirror reflectivity.

3. Results and Discussion

3.1 Near IR overview spectrum of H_2S using FT-IBBCEAS

Before matching frequency comb lines with absorption features of H_2S, its near IR spectrum was measured in the region between 6000 and 6600 cm^{-1} using Fourier-transform incoherent broad-band cavity enhanced absorption spectroscopy (FT-IBBCEAS) [27-29]. FT-IBBCEAS is an approach to measure broadband cavity-enhanced spectra in the NIR region with high resolution [30-32]. The spectrum was measured at a static H_2S pressure of ca. 3 mbar with an integration time of 60 min and a spectral resolution of 0.08 cm^{-1} (cavity length 644 cm, mirror reflectivity $R \approx 0.9998$); for more details concerning the experimental setup see Ref [30]. The line positions obtained agreed with those in HITRAN [33] and the Pacific Northwest National Laboratory (PNNL) data base [34] to within the resolution of the instrument. Fig. 2 shows the overview spectrum of the 2.5 polyad of H_2S (asymmetric top, point group C_{2v}) containing features of 5 combination overtone bands $\nu_1+3\nu_2$, $3\nu_2+\nu_3$, $2\nu_1+\nu_2$, $\nu_1+\nu_2+\nu_3$, and $\nu_2+2\nu_3$. The spectrum is subject

to resonance interactions between all states in this polyad. The same region was spectroscopically studied previously by Ulenikov et al. [35]. The $\nu_1+\nu_2+\nu_3$ (asymmetric) and $2\nu_1+\nu_2$ (symmetric) bands, centered at ~6289.17 cm^{-1} and ~6288.14 cm^{-1} exhibits, are the strongest combination bands with clearly visible and overlapping P, Q and R ro-vibrational components; cf. Fig. 2. The bands $\nu_1+3\nu_2$ and $3\nu_2+\nu_3$, are significantly weaker and especially the very weak combination overtone $\nu_2+2\nu_3$ is negligible for detection applications. A transition in the R branch at ~6339.868 cm^{-1} was used before by Modugno et al. [36] for detection of H_2S at the parts per million level (~4 ppmv) using two-tone frequency modulation spectroscopy. More recently also Chen et al. [26] used R-branch lines of $\nu_1+\nu_2+\nu_3$ at ~6362.88 cm^{-1} for off-axis integrated cavity output spectroscopy.

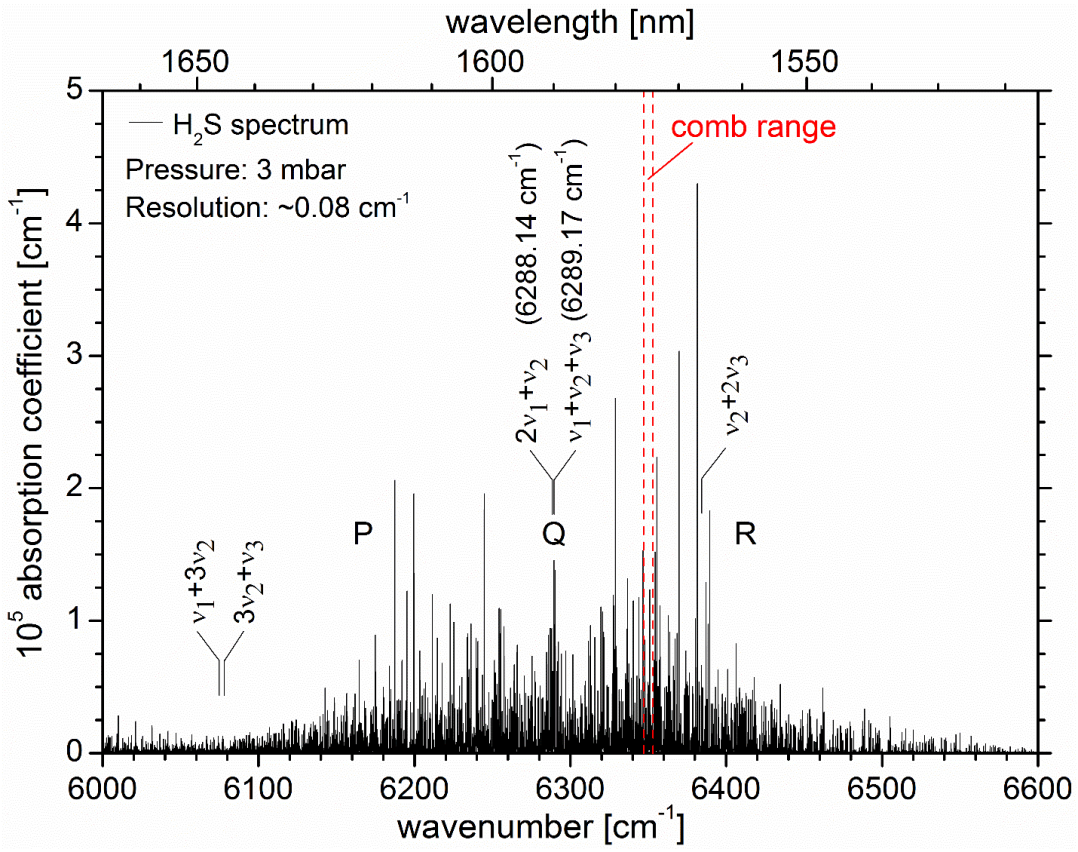

Fig. 2 The near IR absorption spectrum of H_2S at 3 mbar recorded using FT-IBBCEAS with a resolution 0.08 cm^{-1}. The region between 6000 and 6600 cm^{-1} is part of the v = 2.5 polyad. The two dashed vertical lines (red) in the R-branch of the $\nu_1+\nu_2+\nu_3$ and $2\nu_1+\nu_2$ combination bands of H_2S indicate the spectral region where the GSFC (20 lines) is located. Other band centers of weaker overtones in the region are also indicated.

3.2 GSFC application to cavity-enhanced H_2S detection around 6350 cm^{-1}

Owing to the limited tunability of the GSFC, ro-vibrational R-branch transitions of the $\nu_1+\nu_2+\nu_3$ combination band were used in this study to detect H_2S in the region around 6350 cm^{-1}, i.e. in the spectral region indicated by two vertical red lines in Fig. 2. Matching comb lines with H_2S absorption features turned out to be cumbersome as the FWHM of the absorption lines (as well as the FC line widths) are smaller than the spectral resolution of the detection setup.

The HITRAN database [33] gives the H_2S FWHM self-broadening and air-broadening coefficients at 296 K as ~0.316 cm^{-1} atm^{-1} and ~0.148 cm^{-1} atm^{-1}, respectively (with negligible pressure shift). Since the overview spectrum in Fig. 2 was measured at ~3 mbar of H_2S at room temperature, pressure broadening was negligible (<0.001 cm^{-1}) and the expected FWHM due to Doppler broadening at 296 K was $f_G \sim 0.013$ cm^{-1}. Thus the observed FWHM of the absorption lines in Fig. 2 were limited by the resolution of the FTS of 0.08 cm^{-1}.

The situation was similar for H_2S detection with the GSFC in the static gas, where the same FTS was used in conjunction with the short optical cavity. The GSFC experiments were performed at ~82 mbar total pressure where the expected FWHM of absorption lines due to pressure broadening was f_L~0.012 cm^{-1} [33] (see also discussion below)[#1]. The value of f_L is approximately the same size as the expected FWHM Doppler limit of 0.013 cm^{-1} leading to an anticipated Voigt FWHM of $f_V \approx 0.5346 f_L + \sqrt{0.2166 f_L^2 + f_G^2} = 0.021\,\mathrm{cm}^{-1}$ [37]. Even though the comb lines possess a small band width of only ≈10^{-5} cm^{-1} [23], and even though the absolute comb position could be finely tuned in relative steps of ~0.004 cm^{-1}, it was very cumbersome to overlap of comb lines with H_2S absorption lines, because all cavity transmission spectra were measured with the limited spectral resolution of the FTS of 0.08 cm^{-1} (i.e. approximately 3-4 times the FWHM of the

[#1]The true the mixing ratio in the cavity was 0.92 ppTv and hence the partial pressure of H_2S in the cavity was ca. 1 mbar (as will be shown below) and therefore the solely pressure broadened FWHM was expected to be

$$f_L(p) \approx \gamma_{air}\,(1\ \mathrm{atm})[\,p - p_{self}\,] + \gamma_{self}\,(1\ \mathrm{atm})\,p_{self} \approx 0.012\ \mathrm{cm}^{-1}. \quad (2)$$

based on HITRAN broadening coefficients mentioned in the text.

expected absorption lines).[#2] Therefore software was written that identifies the required FSR and optimum GSFC center position (arbitrarily chosen as the position of line 8 – see Fig. 3) to match as many comb lines as possible with absorption features in the relevant spectral region (see Fig. 2). In the software the GSFC spectrum was treated as a series of delta functions, owing to the small bandwidth of $\approx 10^{-5}$ cm^{-1} (300 kHz) per comb line [23]. Using the measured H_2S spectrum in Fig. 2 the matching of up to three comb lines within experimental uncertainty was predicted for a center position of 6349.4 cm^{-1} (position of comb line 8) and an FSR of 10 GHz (~0.334 cm^{-1}). The comb's center position (line 8) was first coarsely tuned several times between ~6349.15 and ~6349.45 cm^{-1} (this range corresponds approximately to the FSR of the GSFC). Where the largest intensity reduction on comb line 3 was observed in the coarse tuning, the comb's center position (line 8) was then finely tuned in steps of 0.004 cm^{-1} (0.001 nm), i.e. from 6349.375 to 6349.415 cm^{-1}. For a comb center position at 6349.407 cm^{-1} (line 8) the best overlap between comb line 3 (at 6347.7487 cm^{-1}) and comb line 9 (at 6349.7532 cm^{-1}) with absorption features of H_2S was obtained;

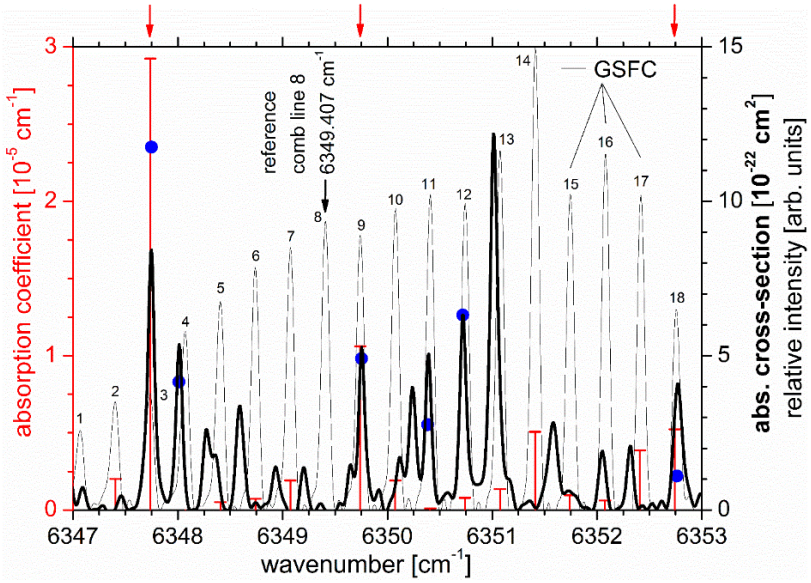

Fig. 3 The thick black trace is a small spectral segment of the H_2S reference spectrum in Fig. 2 which has been scaled at 6350.71 cm^{-1} to the HITRAN absorption cross-sections (=blue solid dots) for a spectral resolution of 0.08 cm^{-1} (bold axis title, right axis). The thin black trace shows 18 comb lines of the GSFC laser (relative intensity; second title on the right axis). The red trace (left axis) shows the absorption coefficient measured on the 18 comb lines for a center position of the GSFC at 6349.407 cm^{-1} and a comb line spacing of 10 GHz. The red vertical arrows indicate comb lines which overlap significantly with H_2S absorption features at 6347.74, 6349.74, and 6352.74 cm^{-1}.

[#2] Note that using the same FT-spectrometer for FT-IBBCEAS and comb experiments has however the advantage potential wavenumber calibration discrepancies are essentially eliminated.

199

200 Fig. 3 illustrates the situation. The thick black trace in Fig. 3 is a small spectral segment of the H_2S
201 reference spectrum in Fig. 2, which has been scaled at 6350.71 cm^{-1} ($\nu_1+\nu_2+\nu_3$; $4_{22}–3_{21}$) to the
202 HITRAN absorption cross-sections represented by the blue solid dots. The HITRAN cross-section
203 have been evaluated for a spectral resolution of 0.08 cm^{-1} and are only shown for the strongest
204 lines in this spectral region. The cross-section values are shown on the right axis (bold axis title).
205 The thin black trace shows the relative intensity of 18 comb lines of the GSFC, only the position
206 of the comb lines is of relevance here. The red trace (left axis) shows the absorption coefficient
207 measured on the 18 comb lines (discussed below) when the comb line spacing (FSR) was 10 GHz
208 and the center position of the GSFC (line 8) was at 6349.407 cm^{-1}. As mentioned above, for these
209 conditions comb lines 3 and 9 overlap well with H_2S absorption features at 6347.7487 cm^{-1}
210 ($\nu_1+\nu_2+\nu_3$; $5_{24}–4_{23}$) and 6349.7532 cm^{-1} ($\nu_1+\nu_2+\nu_3$; $7_{17}–6_{06}$), respectively. Comb line 18 also
211 overlaps significantly with an absorption feature at 6352.74 cm^{-1} ($\nu_1+\nu_2+\nu_3$; $8_{27}–8_{08}$); these three
212 lines are marked with red vertical arrows in Fig. 3.

213 The spectral separation between the peak absorptions at comb line 3 (at 6347.7487 cm^{-1}) and comb
214 line 9 (at 6349.7532 cm^{-1}) is 2.00451 cm^{-1}, which is slightly larger than 6*FSR = 2.00133 cm^{-1} of
215 the comb. This leaves a potential discrepancy of 0.0032 cm^{-1}, which is smaller than the smallest
216 tuning step size of 0.004 cm^{-1} of the comb's center and ca. 3 times smaller than the expected
217 FWHM of the H_2S absorption lines at the corresponding wavelengths. The discrepancy was within
218 the measurement accuracy of the setup. Nevertheless, assuming the HITRAN line positions to be
219 correct within 0.001 cm^{-1}, a comb FSR of 0.334085 cm^{-1} (15.87 MHz larger than the 10 GHz used)
220 would have been optimum for matching comb lines 3 and 9 with H_2S absorption lines.

221 In comparison, the spectral separation between the peak absorptions at comb line 3 (at 6347.7487
222 cm^{-1}) and comb line 18 (at 6352.7623 cm^{-1}) is 5.0136 cm^{-1}, which is slightly larger than 15*FSR
223 = 5.0033 cm^{-1} of the comb. The discrepancy of 0.0103 cm^{-1} is more significant than that for lines
224 3 and 9. It corresponds to approximately the HWHM of the expected Voigt profile and is thus in
225 agreement with the observation in Fig. 3, i.e. comb line 18 was not exactly positioned in the
226 absorption line center. In conclusion, the position match of comb line 3, 9 and 18 with H_2S
227 absorption lines will never reach the theoretical optimum. The strongest absorption line at

~6351.08 cm^{-1} was unfortunately not overlapping well with comb line 13 (see Fig. 3) for the given center position of the comb and other multiple matching were also not easily attained.

We arbitrarily used line 8 of the comb to define the comb's center position, since this line also served as a good reference point for the intensity measurement, I_0, without the sample. In the optimum comb position (at 6349.407 cm^{-1}, see Fig. 3) line 8 does not overlap with any H_2S absorption feature, and its peak intensity can be used as "reference intensity", I_0^{ref}, for all other comb lines. Prior to measurements with H_2S the spectrum of the comb transmitted by an empty cavity (evacuated at ~0.1 mbar) was extensively measured and averaged. From this reference measurement intensity ratios r_k for each comb line k and center comb line 8 can be calculated; $r_k = I_{0,k}^{\mathrm{ref}} / I_{0,8}^{\mathrm{ref}}$. For a measurement with H_2S at first the cavity transmission intensities I_k were stability corrected by dividing through the intensities recorded simultaneously by the OSA. Then the ratio r_k was used to evaluate I_0 on a line that matches a H_2S absorption by multiplying r_k by the peak intensity of comb line 8; $I_{0,k} = r_k I_{0,8}$. The absorption coefficient α_k on a matching comb line k can then be calculated from [27, 29]:

$$\alpha_k = \frac{1-R}{d}\left(\frac{r_k I_{0,8}}{I_k} - 1\right) \tag{1}$$

The absorption coefficients for all α_k in Fig. 3 (red trace, left axis) were calculated using eq. (1). For the two most relevant lines 3 and 9 absorption coefficients $\alpha_3(6347.7487\ \mathrm{cm}^{-1}) = 2.93\times10^{-5}\ \mathrm{cm}^{-1}$ and $\alpha_9(6349.7532\ \mathrm{cm}^{-1}) = 1.06\times10^{-5}\ \mathrm{cm}^{-1}$ were determined (using R = 0.993 ± 0.001 and d = 66 cm). Since the H_2S absorption cross-section, $\sigma_3(6347.7487\ \mathrm{cm}^{-1}) = 1.17\times10^{-21}\ \mathrm{cm}^2$ and $\sigma_9(6349.7532\ \mathrm{cm}^{-1}) = 4.91\times10^{-22}\ \mathrm{cm}^2$ are known from the HITRAN database (converted to instrument resolution, blue dots in Fig. 3), the number density, $n = \alpha_k(\tilde{\nu}) / \sigma_k(\tilde{\nu})$, can be calculated. For absorption features on comb lines 3 and 9 we found n_3=2.50×10^{16} cm^{-3} and n_9=2.16×10^{16} cm^{-3}, corresponding to a discrepancy of the number density of ~13.6%. There are several reasons for this discrepancy: (i) The H_2S cross-sections in the HITRAN database have a reported uncertainty of 10% [30] which on two different lines could lead to a max error of 20%. (ii) Even though for this measurement the matching of the comb lines to the maximum of the absorption features on line 3 and 9 was satisfactory, tuning instabilities of

the GSFC may cause the comb lines to be not exactly at the maximum of the absorption feature leading to an uncertainty in the expected relative absorption signals. When the GSFC was tuned in between measurements the reproducibility of the number densities on the different absorption lines is decreased due to this effect. The reason is that signal optimization is done at a spectral resolution of only 0.08 cm^{-1} (limited by the FTS). This impinges on the overall error of the measured number densities as further discussed in section 3.2. (iii) The comb intensity was recorded for ~4 hours continuously and the absolute upper limit of the observed intensity fluctuations was found to be ≈3.3%. Systematic uncertainties that may impinge on the absolute value of the number density are the measured value of the mirror reflectivity (0.1%) and the length of the cavity (0.3%), which are considered negligible in comparison to the uncertainties listed above.

The averaged number density of 2.33×10^{16} cm^{-3} in this measurement corresponds to 0.92 ppTv. This mixing ratio, calculated from the absorption of sample inside the cavity, was a factor of ~35 lower than that initially expected from the partial pressure measured upon sample preparation. For the preparation of H_2S/air gas mixtures a vacuum line with a mixing volume of ~10 dm^3 made of Pyrex glass was set up inside a fume hood because of the hazardous nature of H_2S. For the α_k measurement in Fig. 3 mixtures of H_2S in air were prepared at a ratio of 6:4 at room temperature (assuming no H_2S losses, see below), i.e. the mixing volume was first filled with H_2S at ~400 mbar and then air at a partial pressure of ~600 mbar was added. The mixture was collected for transfer to the cavity setup (Fig. 1) in a small detachable Pyrex glass tube which was connected on one side of the vacuum line via a Teflon valve. The volume of this "transport tube" was ~82 cm^3. As the cavity volume was 998 cm^3 the partial pressures of air and H_2S in the cavity were expected to be 49.3 mbar and 32.9 mbar, respectively (provided there are no losses of H_2S when filling the transfer volume). The latter pressure value corresponds to a mixing ratio of 32.4 ppTv under standard conditions (1 atm, 296 K), which is ca. 35 times larger than the amount of H_2S found in the absorption experiment (see above). The reason for this difference is the significant sample loss *in the mixing chamber* and transfer volume, as both consisted of Pyrex glass causing inherently large wall losses. Due to efficient chemisorption at metal ion sites in the glass the wall losses in the mixing and transport volume are far from negligible. The fractional throughput of H_2S through a Pyrex glass enclosure is known to be approximately 3% [38], corresponding to losses of a factor ~33 in agreement with the loss factor found in the absorption experiment. Although the data in

Ref. [38] are not universal for arbitrary experimental conditions, the low fractional throughput of Pyrex indicates that much less H_2S was collected in the transfer volume. Note that the filling pressure was not measured in the transfer volume itself, but at a distance from it in the larger mixing volume, which was essentially filled with a large excess of air. After the transfer of the sample to the GSFC setup the pressure was measure in the cavity again.

To systematically study the effect of losses in the transfer of gas mixtures from the mixing volume to the cavity, the absorption coefficients were determined on laser lines 3 and 9 for five different H_2S concentrations. For these measurements the mixing volume was initially filled with different partial pressures of H_2S between 100 and 500 mbar, then filled up with air to 1000 mbar, and finally transferred to the cavity in the transfer volume. The absorption coefficients on line 3 and 9 had an overall uncertainty of $\Delta_{max} < 25\%$ (see Table 1; this error is not to be confused with the difference (discrepancy) in the number densities based on measurements on comb line 3 and 9). The maximal uncertainty of 25% is associated with the reproducibility of the measured absorption coefficient per comb line. For each partial pressure of H_2S the absorption coefficient was measured 3-4 times. Between each measurement the GSFC was finely tuned to optimize the signal and to obtain an uncertainty in the reproducibility for a given H_2S concentration, which was evaluated based on a student's t-distribution. Apart from contributions to Δ_{max} that are associated with the uncertainty of the H_2S cross-sections in HITRAN (10%), the optimum position of the comb lines with respect to the absorption maximum was difficult to establish from measurement to measurement as a detection resolution of 0.08 cm^{-1} was used for signal optimization. This resolution is larger than the FWHM of the absorption line at the measurement conditions (~0.021 cm^{-1}) and much larger than the comb line width (~10^{-5} cm^{-1}). The accuracy therefore relied strongly the tuning stability of the GSFC, causing a fluctuation in the absorption coefficient and a discrepancy in the relative absorption coefficients measured on line 3 and 9. The 3σ standard deviation of the absorption coefficient on lines that were not matched perfectly with H_2S absorption features was $\approx 3.6\times10^{-6}$ cm^{-1}. This value of the minimum absorption coefficient in an integration time of 120 s corresponds to ≈680 ppmv, which can be taken as a conservative (upper) limit of detection (LOD) for this approach, because some of the laser lines always overlap to a certain extent with H_2S absorptions, all of which were taken into account in the above stated 3σ LOD. From the H_2S absorption measurements the number densities in the cavity was again

estimated based on HITRAN cross-sections, which were systematically (expectedly) smaller than those estimated from the pressure in the mixing volume due to the losses of H_2S in the transfer process. An expected loss factor of ca. 33 (averaged) was found for comb line 9, while the loss factor appeared to be larger (average ~50) for line 3. This difference corroborates that the comb lines 3 and 9 were not equally well matched to the maximum of a H_2S absorption line. While line 9 was probably near the maximum of the absorption feature (owing to the smaller loss factor), line 3 was positioned off the center of the H_2S absorption line. Within our spectral resolution of only 0.08 cm^{-1} the exact position cannot be independently verified. The fact that the ratio of loss factors is approximately constant for all concentrations indicates that the approach is reproducible within the above stated limits, i.e. the laser position and mode structure enabling the light to be transmitted by the cavity is sufficiently stable in the current approach. The data are summarized in Table 1 and graphically represented in Fig. 4.

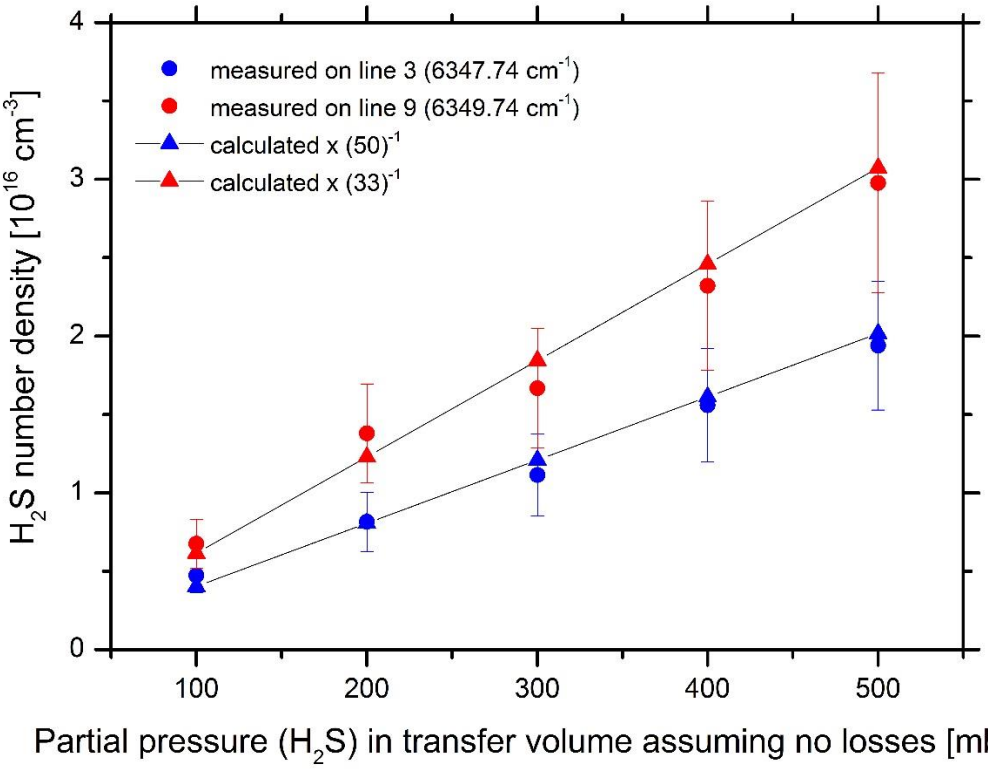

Fig. 4 H_2S number density in the cavity as measured from the absorption coefficient on comb line 3 (blue circles) and line 9 (red circles) vs the alleged partial pressure of H_2S in the mixing volume. The triangular symbols represent the number densities derived from the partial pressures on the horizontal axis, divided by a loss factor of 50 (blue) and 33 (red). They can then be compared with the number densities from the absorption measurement. Error bars refer to the uncertainties stated in column 4 of Table 1.

Table 1 Summary of measurement parameter concerning concentration dependent measurements. Values in Column 4 vs column 1 are shown in Fig. 4 (cirlces). Col 1: Presumed H_2S partial pressure in 10 dm^3 mixing volume without losses, in [mbar], measured with absolute pressure gauge. Col 2: Anticipated number density in the 1 dm^3 cavity based on pressure in Col 1 and a 82 cm^3 transfer volume, assuming no losses. Col 3: Measured absorption coefficient on line 3 and 9. The reproducibility error is 25%. Col 4: Corresponding abs. cross-section from HITRAN database on line 3 and 9. Col 5: Number densities following from values in Col 3 and 4. The error in col 3 is explicitly stated here per value (<25%). Col 6: Ratio of the anticipated number density (if there are no losses, Col 2) and the measured number density from the absorption (Col 5). The values corresponds to the approximate loss factor of H_2S in the transfer process from the mixing volume to the cavity. As a factor of ca. 33 is expected from ref [38]; the higher value on line 3 indicates that the comb line was not exactly matched to the center (i.e. the maximum) of the H_2S absorption feature.

Pressure [mbar]	Number density [10^{17} cm^{-3}]	Absorption coefficient [10^{-6} cm^{-1}]		Absorption cross-section [10^{-22} cm^2]		Number density [10^{13} cm^{-3}] (ppmv)		Number density ratio – loss factor –	
in mixing volume	calculated from pressure	Line 3	Line 9	Line 3	Line 9	Line 3	Line 9	Line 3	Line 9
		Δ_{max} < 25%		From HITRAN (uncertainty 10%)		Measured (Δ_{max} < 25%)		Avg: 50	Avg: 33
100	2.01	5.6	3.3	11.76	4.91	470 ± 100	680 ± 160	43	30
200	4.02	9.6	6.8	11.76	4.91	820 ± 190	1380 ± 320	49	29
300	6.03	13.1	8.2	11.76	4.91	1110 ± 260	1670 ± 380	54	36
400	8.04	18.3	11.4	11.76	4.91	1560 ± 360	2320 ± 530	52	35
500	10.05	22.8	14.6	11.76	4.91	1940 ± 450	2980 ± 680	52	34

Fig. 4 shows, on the horizontal axis, the partial pressure of H_2S as measured in the mixing volume. On the vertical axis the number densities inside the cavity are shown (circular symbols). They were determined from the absorption coefficient measured on line 3 (blue data points) and line 9 (red data points) for the respective mixing partial pressures. The error bars refer to the circular symbols. Additionally displayed are the number densities (triangular symbols, straight black line, no error bars) as they would be expected from the partial pressures, divided by the average loss factor for H_2S for the corresponding line (50 for line 3 and 33 for line 9; cf. Table 1). Fig. 4 illustrates the consistency of Table 1 for measurement at different concentrations.

The first value in Fig. 4 (100 mbar) is essentially the detection limit. The lower explosion limit (LEL) of H_2S in air is ~4% while the upper explosion limit (UEL) is ~44% [39]. Since the LOD of ~0.7 per mille by volume is significantly smaller than the lower explosion limit (LEL) [39], the GSFC measurements presented here are well sufficient to detect H_2S at its LEL even in the near infrared.

Finally, an attempt was made to corroborate our results in Figs. 3 & 4 through the measurement of a high resolution line spectrum, by recording absorption coefficients on line 3 while stepping the

center of the GSFC over the optimum position at 6349.407 cm^{-1} (line 8 in Fig. 3) in steps of 0.004 cm^{-1}. The problem with this experimental line width test was that all absorption measurements were taken with a resolution of 0.08 cm^{-1}, and the true position of the laser with respect to the line center of the absorption line at 6347.74 cm^{-1} (line 3) could not be determined with sufficient accuracy. The test measurement relied solely on the tuning stability of master laser. Even though the spectrum of the line at 6347.74 cm^{-1} could be recorded by tuning the GSFC, the FWHM was ca. half the size of the anticipated Voigt FWHM (0.021 cm^{-1}) according to the estimated pressure and Doppler broadening, see above. This discrepancy is likely to be a consequence of the electronic tuning stability and potential small drifts of the GSFC. The stability was investigated by independently tuning to the GSFC center position to the maximum absorption signal many times in the context of the I_0 measurements. The absolute laser position, as solely determined from the tuning voltage, could be reproduced within 0.017 cm^{-1}, which is 20% smaller than the anticipated FWHM of the expected H_2S absorption line. The tuning to the maximum position is uncertain within that limit, explaining the different loss factors found for the laser comb lines 3 and 9.

4. Conclusions and outlook

Two comb lines (3 and 9) were matched to absorption lines of H_2S in the near infrared L-band without locking the laser to the cavity mode structure. Without locking the laser line, the overlap of the laser with the absorption features was accurate and stable to within ≈80% of the FWHM of the absorption line. From the non-resonant comb lines, an rms noise equivalent absorption for this approach of approximately 3.9×10^{-5} cm^{-1} $Hz^{-1/2}$ was found, which corresponds to a detection limit of ca. 700 ppmv of H_2S in 120 s. This sensitivity is well below the lower explosion limit of H_2S of 4% and was achieved with a very modest finesse (~450) cavity.

Future work will focus on making the setup more compact by using custom-designed integrated combs and improving the detection resolution through a dual comb approach. Alternative coupling scheme of the laser to the cavity will be looked into and the detection cell is to be developed into a flow cell. Other spectral regions are to be targeted.

Acknowledgement

The support by Science Foundation Ireland's (SFI) TIDA Programme (14/TIDA/2415) is gratefully acknowledged. Enterprise Ireland (EI) is also providing financial support under the Technology Innovation Development Award scheme, Commercialisation Fund (CF 2017 0683B). We would like to thank Prof Frank Peters and Prof John McInerney for the loan of an OSA for this project. We are grateful to Mr Christy Roche and Mr Joe Sheehan for their excellent technical assistance.

References

[1] J. Ye, S.T. Cundiff (Eds.), *Femtosecond Optical Frequency Comb: Principle, Operation, and Applications*, (Kluwer Academic Publishers/Springer, Norwell MA, 2005)

[2] T. W. Hänsch, Nobel lecture: Passion for precision. Rev. Mod. Phys. **78,** 1297–1309 (2006).

[3] J. L. Hall, Nobel lecture: Defining and measuring optical frequencies. Rev. Mod. Phys. **78,** 1279–1295 (2006)

[4] S.A. Diddams, The evolving optical frequency comb. J. Opt. Soc. Am. B **27,** B51–B62 (2010)

[5] N.R. Newbury, Searching for applications with a fine-tooth comb. Nat. Photonics **5,** 186–188 (2011)

[6] T.W. Hänsch, N. Picqué, Laser spectroscopy and frequency combs. J. Phys. Conference Series **467,** 012001 (2013)

[7] F. Adler, M.J. Thorpe, K.C. Cossel, J. Ye, Cavity-enhanced direct frequency comb spectroscopy: Technology and applications. Annu. Rev. Anal. Chem. **3,** 175–205 (2010)

[8] S.A. Diddams, L. Hollberg, V. Mbele, Molecular fingerprinting with the resolved modes of a femtosecond laser frequency comb. Nature **445,** 627–630 (2007)

[9] L. Nugent-Glandorf, T. Neely, F. Adler, A.J. Fleisher, K.C. Cossel, B. Bjork, T. Dinneen, J. Ye, S.A. Diddams, Mid-infrared virtually imaged phased array spectrometer for rapid and broadband trace gas detection. Opt. Lett. **37,** 3285–3287 (2012)

[10] C. Gohle, B. Stein, A. Schliesser, T. Udem, T.W. Hänsch, Frequency comb vernier spectroscopy for broadband, high-resolution, high-sensitivity absorption and dispersion spectra. Phys. Rev. Lett. **99,** 263902 (2007)

[11] R. Grilli, G. Méjean, C. Abd Alrahman, I. Ventrillard, S. Kassi, D. Romanini, Cavity-enhanced multiplexed comb spectroscopy down to the photon shot noise. Phys. Rev. A **85,** 051804 (2012)

[12] J. Mandon, G. Guelachvili, N. Picqué, Fourier transform spectroscopy with a laser frequency comb. Nat. Photonics **3,** 99–102 (2009)

[13] F. Adler, P. Masłowski, A. Foltynowicz, K. C. Cossel, T. C. Briles, I. Hartl, J. Ye, Mid-infrared Fourier transform spectroscopy with a broadband frequency comb. Opt. Express **18,** 21861–21872 (2010)

[14] B. Bernhardt, A. Ozawa, P. Jacquet, M. Jacquey, Y. Kobayashi, T. Udem, R. Holzwarth, G. Guelachvili, T. W. Hänsch, N. Picqué, Cavity-enhanced dual-comb spectroscopy. Nature Photonics **4**, 55–57 (2010)

[15] M. Zeitouny, P. Balling, P. Křen, P. Mašika, R.C. Horsten, S.T. Persijn, H.P. Urbach, N. Bhattacharya, Multi-correlation Fourier transform spectroscopy with the resolved modes of a frequency comb laser. Ann. Phys. **525,** 437–442 (2013)

[16] A. Khodabakhsh, A.C. Johansson, A. Foltynowicz, Noise-immune cavity-enhanced optical frequency comb spectroscopy: a sensitive technique for high-resolution broadband molecular detection. Appl. Phys. B **119,** 87–96 (2015)

[17] A.J. Fleisher, D.A. Long, Z.D. Reed, J.T. Hodges, D.F. Plusquellic, Coherent cavity-enhanced dual-comb spectroscopy. Opt. Express **24,** 10424–10434 (2016)

[18] I. Coddington, N. Newbury, W. Swann, Dual-comb spectroscopy. Optica **3,** 414–426 (2016)

[19] T. Gherman, D. Romanini, Mode–locked cavity–enhanced absorption spectroscopy. Opt. Express **10,** 1033–1042 (2002)

[20] A. Foltynowicz, P. Masłowski, A.J. Fleisher, B.J. Bjork, J. Ye, Cavity-enhanced optical frequency comb spectroscopy in the mid-infrared application to trace detection of hydrogen peroxide. Appl. Phys. B **110,** 163–175 (2013)

[21] M. J. Thorpe, J. Ye, Cavity-enhanced direct frequency comb spectroscopy, Appl. Phys. B **91,** 397–414 (2008)

[22] P. M. Anandarajah, R. Maher, Y. Xu, S. Latkowski, J. O'Carroll, S.G. Murdoch, R. Phelan, J. O'Gorman, L.P. Barry, Generation of coherent multicarrier signals by gain switching of discrete mode lasers. IEEE Photonics J. **3,** 112 (2011)

[23] P. Anandarajah, R. Zhou, R. Maher, M.D. Guitérrez-Pascual, F. Smyth, V. Vujicic, L.P. Barry, Flexible optical comb source for super channel systems. Optical Fiber Communication Conference, Proceedings Paper# OTh3I.8, Anaheim CA, USA (2013)

[24] M.D. Guitérrez, J. Braddell, F. Smyth, L. P. Barry, Monolithically integrated 1´4 comb de-multiplexer based on injection locking. 18th European Conference on Integrated Optics, Proceedings Paper# ECIO-p37, Warsaw, Poland (2016)

[25] B. Jerez, P. Martín-Mateos, E. Prior, C. de Dios, P. Acedo, Dual optical frequency comb architecture with capabilities from visible to mid-infrared. Opt. Express **24,** 14986–14994 (2016)

[26] W. Chen, A.A. Kosterev, F.K. Tittel, X. Gao, W. Zhao, H_2S trace concentration measurements using off-axis integrated cavity output spectroscopy in the near-infrared. Appl. Phys. B **90,** 311–315 (2008)

[27] S.E. Fiedler, A. Hese, A.A. Ruth, Incoherent broadband cavity-enhanced absorption spectroscopy. Chem. Phys. Lett. **371,** 284–294 (2003)

[28] A.A. Ruth, J. Orphal, S.E. Fiedler, Cavity enhanced Fourier transform absorption spectroscopy using an incoherent broadband light source. Appl. Opt. **46,** 3611–3616 (2007)

[29] J. Orphal, A.A. Ruth, High-resolution Fourier-transform cavity-enhanced absorption spectroscopy in the near-infrared using an incoherent broad-band light source. Opt. Express **16,** 19232–19243 (2008)

[30] D.M. O'Leary, A.A. Ruth, S. Dixneuf, J. Orphal, R. Varma, The near infrared cavity-enhanced absorption spectrum of methylcyanide. J. Quant. Spectr. Rad. Trans. **113,** 1138–1147 (2012)

[31] R. Raghunandan, A. Perrin, A.A. Ruth, J. Orphal, First analysis of the $2\nu_1+3\nu_3$ band of NO_2 around 7192 cm^{-1}. J. Mol. Spectrosc. **297,** 4–10 (2014)

[32] S. Chandran, R. Varma, Near infrared cavity enhanced absorption spectra of atmospherically relevant ether-1,4-dioxane. Spectrochim. Acta A: Mol. Biomol. Spectr. **153**, 704–708 (2016)

[33] L.S. Rothmana, I.E. Gordon, Y. Babikov, A. Barbe, D. Chris Benner, P.F. Bernath, M. Birk, L.Bizzocchi, V.Boudon, L.R. Browni, A. Campargue, K. Chance, E.A. Cohen, L.H.Coudert, V.M. Devi, B.J.Drouin, A. Fayt, J.-M. Flaud, R.R. Gamachem, J.J. Harrison, J.-M. Hartmann, C. Hill, J.T. Hodges, D. Jacquemart, A. Jolly, J. Lamouroux, R.J. LeRoy, G. Li, D.A. Long, O.M. Lyulin, C.J. Mackie, S.T. Massie, S. Mikhailenko, H.S.P. Müller, O.V. Naumenko, A.V. Nikitin, J. Orphal, V. Perevalov, A. Perrin, E.R. Polovtseva, C. Richard, M.A.H. Smith, E. Starikova, K. Sung, S. Tashkun, J.Tennyson, G.C. Toon, V.G. Tyuterev, G. Wagner, The HITRAN 2012 molecular spectroscopic database. J. Quant. Spectr. Rad. Trans. **130,** 4–50 (2013)

[34] S.W. Sharpe, T.J. Johnson, R.L. Sams, P.M. Chu, G.C. Rhoderick, P.A. Johnson, Gas-phase databases for quantitative infrared spectroscopy. Appl. Spectrosc. **58,** 1452–1461 (2004)

[35] O.N. Ulenikov, A.-W. Liu, E.S. Bekhtereva, O.V. Gromova, L.-Y. Hao, S.-M. Hu, High-resolution Fourier transform spectrum of H_2S in the region of the second hexade. J. Mol. Spectrosc. **234,** 270–278 (2005)

[36] G. Modugno, C. Corsi, M. Gabrysch, M. Inguscio, Detection of H_2S at the ppm level using a telecommunication diode laser. Opt. Com. **145,** 76–80 (1998)

[37] J.J. Olivero, R.L. Longbothum, Empirical fits to the Voigt line width: A brief review. J. Quant. Spectr. Rad. Trans. **17,** 233–236 (1977)

[38] W.C. Kuster, P.D. Goldan, Quantitation of the losses of aqueous sulfur compounds to enclosure wall, Env. Sci. Technol. **21,** 810–815 (1987)

[39] M.G. Zabetacis, Flammability characteristics of combustible gases and vapors, Bulletin 627, US Department of the Interior, Bureau of Mines (1965)